Supplementary materials

for

Persistent millennial-scale glacier fluctuations during the last glacial cycle in the southern Tibetan Plateau

Guocheng Dong[1, 2 *], Weijian Zhou[1, 2], Yunchong Fu[1, 2], Feng Xian[1, 2], Li Zhang[1, 2]

[1] State Key Laboratory of Loess Science, Institute of Earth Environment, Chinese Academy of Sciences, Xi'an 710061, China

[2] Shaanxi Key Laboratory of Accelerator Mass Spectrometry Technology and Application, Xi'an AMS Center of IEECAS & Xi'an Jiaotong University, Xi'an 710061, China

[*]Corresponding author: donggc@ieecas.cn

This PDF file includes:

Background

Dating results and interpretation

Comparison of outlier detection results from three commonly-used methods

Uncertainties in moraine age determination

Estimation of the response time of the studied glaciers

Correlation of the identifed glacial events with sea surface temperatures (SSTs) in the Indio-Pacific Warm Pool (IPWP)

Supplementary Figures 1, 2, 3, 4, 5, 6, and 7

Supplementary Tables 1, 2, and 3

Background

The WNM is a roughly northeast-southwest trending mountain range in the southern TP (Fig. 1A). Elevations across this ~250-km-long mountain range are primarily over 5000 m asl, with the highest summit (Mt. Nyainqentanglha) peaking at 7162 m asl (Fig. 1B). The bedrock of WNM mainly consists of Cretaceous-Tertiary granitoid and orthogneiss as well as metasedimentary lithology ranging in age from Paleozoic to Cretaceous[1, 2]. Climates in this region are dominated by the ISM in summer and the northern mid-latitude westerlies in winter[3, 4]. At seven meteorological stations surrounding the WNM, the mean annual precipitation amounts from 2005 to 2008 measured 377–500 mm[4]. The mean annual air temperature was recorded to vary between -0.6 and 2.9 ºC[4].

Our study is centered in the confluence area of the Anzhongqu and Sibuqu valleys, which are situated in the southwestern-most part of the WNM (Fig. 1B). The Anzhongqu Valley stretches south-eastward for ~6 km to an elevation of around 4770 m asl, where it merges into the ~14-km-long east-draining Sibuqu Valley (Fig. 2A). From there on, the valley presents an asymmetric cross-valley profile downstream, with a relatively steep left-lateral (northern) flank and a gentler right-lateral (southern) flank (Fig. 2A). Along the right-lateral flank, four sets of moraine remnants can be distinguished between the valley confluence and the mountain front area (Fig. 2 and Supplementary Fig. 1). At present, patchy cirque glaciers occupy an area of <0.5 km^2 in the studied catchment (Fig. 2A). These glaciers terminate between elevations of 5520–5740 m asl.

The earliest glacial geomorphic study in this area was conducted by Kuhle[5], formulating the TP ice-sheet hypothesis that is endorsed by a follow-up study[6]. More detailed geomorphic studies were implemented at the beginning of the 21st century based on the morpho-stratigraphic relationship of moraines[7-11]. Despite lacking direct chronological evidence, these studies argued against the ice-sheet viewpoint by defining multiple glacial events that spanned the last two glacial cycles.

Following these studies, Wu et al.[12] provided the first absolute age controls in the mountain front areas between Damshung and Yanbajain (Fig. 1B) by employing optically stimulated luminescence, electron spin resonance, and U-series dating techniques. The authors ascribed five sets of glacial and associated sediments to the middle and late Pleistocene. After that, Owen et al.[13] presented ^{10}Be data, for the first time, in the WNM region, building a chronological framework for the last glacial and deglacial periods in the Barenlong Valley (site 7 in Fig. 1B). They point to that the WNM glaciers reached their maximum extent of the last glaciation before Marine Isotope Stage 2 (MIS 2)[14] and the Last Glacial Maximum (LGM; 19.0–26.5 ka[15]), inconsistent with Northern Hemisphere ice sheets. The authors also ascribed a post-LGM advance to HS1. Their findings are subsequently confirmed by ^{10}Be-based moraine chronologies established in five valleys (sites 2–6 in Fig. 1B)[16–19]. More recently, four moraines in the Mt. Kuoqionggangri area (sites 8 and 9 in Fig. 1B) were dated to the latest Little Ice Age by Xu et al.[20].

In addition, glacier-climate modeling was also widely carried out across the WNM[17, 19–23], which were mostly centered in the aforementioned ^{10}Be dating sites. These modeling studies, in conjunction with chronological research, provide us a broad context to examine the last glacial history of WNM glaciers.

Dating results and interpretation

Beginning with the innermost, and hence youngest, moraine (M1) dated here, six glacial boulders produced exposure-ages ranging from 19.0 ± 0.5 ka to 19.9 ± 0.6 ka (Supplementary Table 1). These ages display an approximately normal distribution, forming a tight cluster around 19.3 ka (Supplementary Fig. 2A). This confirms the outlier detection results; that is, no outlier has been found by the 1σ-level method. These internally consistent ages average 19.3 ± 0.3 ka (Supplementary Fig. 2A).

Five exposure-ages obtained from the M2 moraine have a range of 19.9 ± 0.4–22.7 ± 0.6 ka (Supplementary Table 1). At the 1σ level, the oldest age is not overlapping with the other four that are closely grouped around 20.1 ka (Supplementary Fig. 2B). Also, the age is significantly older than those provided by the older M3 moraine, thereby being out of morphostratigraphic order. These convince us to reject sample 19D12 as a boulder with nuclide inheritance. The resultant subset returns a moraine mean of

20.1 ± 0.2 ka.

The M3 moraine afforded ^{10}Be ages that are between 20.4 ± 0.5 ka and 20.7 ± 0.5 ka (n = 10). These ten exposure-ages are well clustered around 20.6 ka, exhibiting a high level of internal consistency (Supplementary Fig. 2C), so that no outlier has been statistically identified. These nearly identical ages yield an arithmetic mean of 20.6 ± 0.1 ka.

A total of forty-four boulders were dated on the moraine complex (M4). With regard to the innermost M4$_A$ ridge, six boulders gave exposure-ages having a range of 19.6 ± 0.4–21.9 ± 0.4 ka (Supplementary Table 1). Among those ages, five are internally indistinguishable, clustering together around 21.6 ka (Supplementary Fig. 2D). The remaining age (19.6 ± 0.4 ka) is younger than most ages from the inboard M3 moraine, and is hence stratigraphically discordant. We assume incomplete exposure, which could result from moraine denudation, boulder toppling, and sediment/snow cover, might have affected this boulder. Removal of the morphorstratigraphic outlier leads to an age group with an arithmetic mean of 21.6 ± 0.2 ka.

Samples from boulders on the outboard moraine ridge (M4$_B$) were dated to 24.8 ± 0.4–29.9 ± 0.4 ka (n = 12; Supplementary Table 1), with most (n = 8) of which lying within the early stage of LGM (Fig. 3E). These eight ages agree well with each other within the 1σ analytical uncertainties and generate a dominant distribution peaking at 25.1 ka, whereas the other four older ages form a secondary and less well-expressed peak (Supplementary Fig. 2E). Based on the 1σ-level approach, we treated these four ages as potential outliers, which brings the moraine mean to 25.1 ± 0.2 ka. These four apparently older anomalies may have reflected boulders incorporated from the the earlier 28.9 ± 0.9 ka advance, as previously suggested for boulders deposited advances with similar extent[24].

Thirteen glacial boulders atop the next outboard ridge (M4$_C$) afforded a relatively broad spread of ages ranging between 22.3 ± 0.9 ka and 37.8 ± 0.6 ka (Fig. 2B). These ages show a bimodal distribution, with a dominant distribution (n = 8) peaking at 29.2 ka and a younger secondary mode (n = 3) being around 26.2 ka. Following the 1σ-level strategy, we regard the oldest one and youngest four ages as potential outliers (Fig.

3F). The oldest one is > 2σ older than the mean of the remaining ^{10}Be ages, representing a boulder sample with inherited ^{10}Be nuclides[25]. Rather, the apparently youngest four samples, despite showing no signs of surface weathering, might have experienced boulder toppling after their emplacement on moraine ridge. The remaining population affords an arithmetic mean of 28.9 ± 0.9 ka.

Finally, the outermost two moraine ridges, $M4_D$ and $M4_E$, yielded relatively clustered exposure-ages (Supplementary Figs. 2G and 2H) that fall well within the late-MIS 3 time interval (Figs. 3G and 3H). The youngest and oldest exposure-ages given by $M4_D$ are not in morpho-stratigraphic order, testifying to the statistical results returned by the 1σ-level strategy (Fig. 3G). Likewise, the apparently oldest boulder (19D24) dated on $M4_E$ is excluded from the mean age calculation as well (Fig. 3H). In this way, the two outlier-free distributions return moraine means of 34.1 ± 0.4 ka ($M4_D$) and 35.3 ± 0.4 ka ($M4_E$), respectively.

Comparison of outlier detection results from three commonly-used methods

Despite being a widely-adopted method adhered to strict rules, the '1σ-level' strategy remains subjective in some ways. We thus compare its performance against two additional routinely-used approaches, Probabilistic Cosmogenic Age Analysis Tool (P-CAAT)[26] and Peirce's criterion[27],which have been widely used to identify potential outliers for ^{10}Be exposure dating of moraine boulders[28, 29].

The P-CAAT program provided entirely consistent results with the '1σ-level' technique (Supplementary Table 4), identifying fourteen potential outliers in total. These include one sample (19D19) from M2, one (19D37) from M4, four (19D42, 45, 46, and 49) from $M4_A$, five (19D54, 56, 58, 59, and 62) from $M4_C$, two (19D29 and 34) from $M4_D$, and one (19D24) from $M4_E$ (Supplementary Fig. 3). Peirce's criterion, regardless of uncertainties in age, releases coherent outlier identification results for most moraines, with exception of $M4_B$ and $M4_C$. No anomalies have been found on $M4_B$; and the apparently oldest sample (19D62) on $M4_C$ was regarded as an outlier. That is, the criterion finds less number of outliers on these two moraines as compared with the '1σ-level' and P-CAAT methods (Supplementary Table 4). These two approaches impose a more critical threshold by taking error in AMS measurements (internal age uncertainties) into account, pinpointing cause that makes such a difference. More importantly, these two techniques result in moraine means that agree well with the relative position of moraines (Supplementary Fig. 4). These convince us to adopt the consistent outlier-detection results of these two approaches to discuss moraine chronologies in this study.

Uncertainties in moraine age determination

Uncertainties in moraine ages are crucial to comparison of millennial-scale glacial events identified here with high-frequency climate signals. Such uncertainties can result from production-rate datasets and scaling models used to calculated exposure-ages. Here, we assess the sensitivity of these two interpretations on moraine age determination. We first compare exposure-ages calculated using three scaling models[30–33] (Supplementary Table 1) on the basis of Northern Hemisphere production-rate calibrations at mid-latitude and high-altitude[34, 35] (hereafter the SP production-rate dataset). We then compare the LSDn[30] results given by the SP and default (global)[36] production-rate datasets.

We find that the time-independent St model produces ages having values of up to 9% higher than the LSDn model used here. Note, however, that the St mdoel is based on an assumption of constant ^{10}Be production rates, conflicting with the fact that ^{10}Be production rates change over time due to secular changes in the Earth's geomagnetic field[37]. In regard to the time-dependent (LSDn and Lm) models, age differences vary between 4% and 5%, comparable to that caused by AMS measurements. As such, each individual exposure ages returned by the time-dependent schemes are indistinguishable at the 1σ level (Supplementary Fig. 5). This also the case with production-rate datasets (Supplementary Fig. 5). Yet, we chose the SP production-rate dataset for the subsequent reasons. First, ^{10}Be production rates vary following changes in both latitude and altitude. The SP calibration dataset is located at a similar latitude in northern hemisphere to our WNM site, implying the most precise exposure-ages from our current knowledge. Second, some controversial production-rate calibrations are included by the default production-rate dataset[38]. So in closing, we choose the LSDn results calculated using the SP production-rate dataset to discuss glacial events and climatic driving mechanism.

Estimation of the response time of the studied glaciers

Here, we used the approach developed by Jóhannesson et al.[39] to assess the response time of different-sized glaciers, which helps us in examining whether the dated moraines represent millennial-scale glacial activities. According to the method, the response time of glaciers is roughly expressed as a ratio of mean ice thickness to glacier mass balance. To calculate the mean ice thickness, we first reconstructed the former glacier surface using a python-based tool[40] for each individual glacial activities within the ArcGIS environment. The ice thickness were then calculated by subtracting the present-day topography from the reconstructed glacier surface. Here, we use a value of 1.067 for glacier mass balance[41, 42] to estimate the response time of glaciers. The estimated value of glacier response time range from 117 to 181 yr (Supplementary Fig. 6), which decreases following the size of glaciers. The results indicate that the dated moraines may reflect millennial-scale rather than annua glacier behaviors.

Correlation of the identifed glacial events with sea surface temperatures (SSTs) in the Indio-Pacific Warm Pool (IPWP)

To examine glacial fluctuations in a broader climate context, we compare millennial-scale glacial behaviors with the north- and south-IPWP SSTs (Supplementary Fig. 7). Evidently, moraine-building events match well in time with the depressed SSTs reconstructed from core SO189-114KL[43] in the northern tropical Indian Ocean (Supplementary Figs. 7A and 7B). Akin to the northern Indian Ocean, an association, although looser, can also be roughly observed for the northwestern Pacific Ocean[44, 45] (Supplementary Figs. 7A and 7C–7D). Yet, this is not the case with the south-IPWP SSTs[43, 46] (Supplementary Figs. 7A and 7E–7F). These differences can be envisioned to zonal seesaw between the southern and northern tropical Indian Ocean as well as the tropical Indian and western Pacific Oceans, as revealed by observational and modelling evidence[47, 48]. The interpretation of zonal seesaw is, however, beyond the scope of our study, so we have not made a more in-depth discussion. Altogether, we propose that the northern tropical Indian Ocean SSTs were likely responsible for millennial-scale glacial events identified here. Also, we elaborate on the potential climate processes that operated during the hypothesized correlation in the main text.

Supplementary Figure 1 Photographs showing selective glacial landforms and associated boulders, together with their exposure-ages and 1σ internal uncertainties. (A) View from the M2 moraine towards the confluence of the Sibuqu and Anzhongqu valleys. Shown in the foreground is the M2 moraine, behind which the morphorgraphically younger M1 moraine is illustrated by white dashed line. (B) North-south perspective of the M2 moraine, which is annotated with white dashed lines. The morpho-stratigraphically older moraine M3 is marked by black dashed line in the foreground. (C) Looking westwards (upstream) standing on the M1 moraine. Shown in the foreground is boulder sample numbered 19D19. (D) Eastward view of a ~0.6-m-high boulder (19D11) resting on the M2 moraine. (E) Example of a glacial boulder well-rooted in the M3 moraine. (F) Illustration of a typical bouldery ridge outside of the catchment outlet. Vantage is east. Shown in the foreground is the 19D35 sample collected on the $M4_A$ ridge, which is depicted by the white dashed line. (G) Photograph, with vantage south, showing a ~1-m-high boulder embedded in the outermost bouldery ridge $M4_E$. No prominent glacial features can be observed downstream.

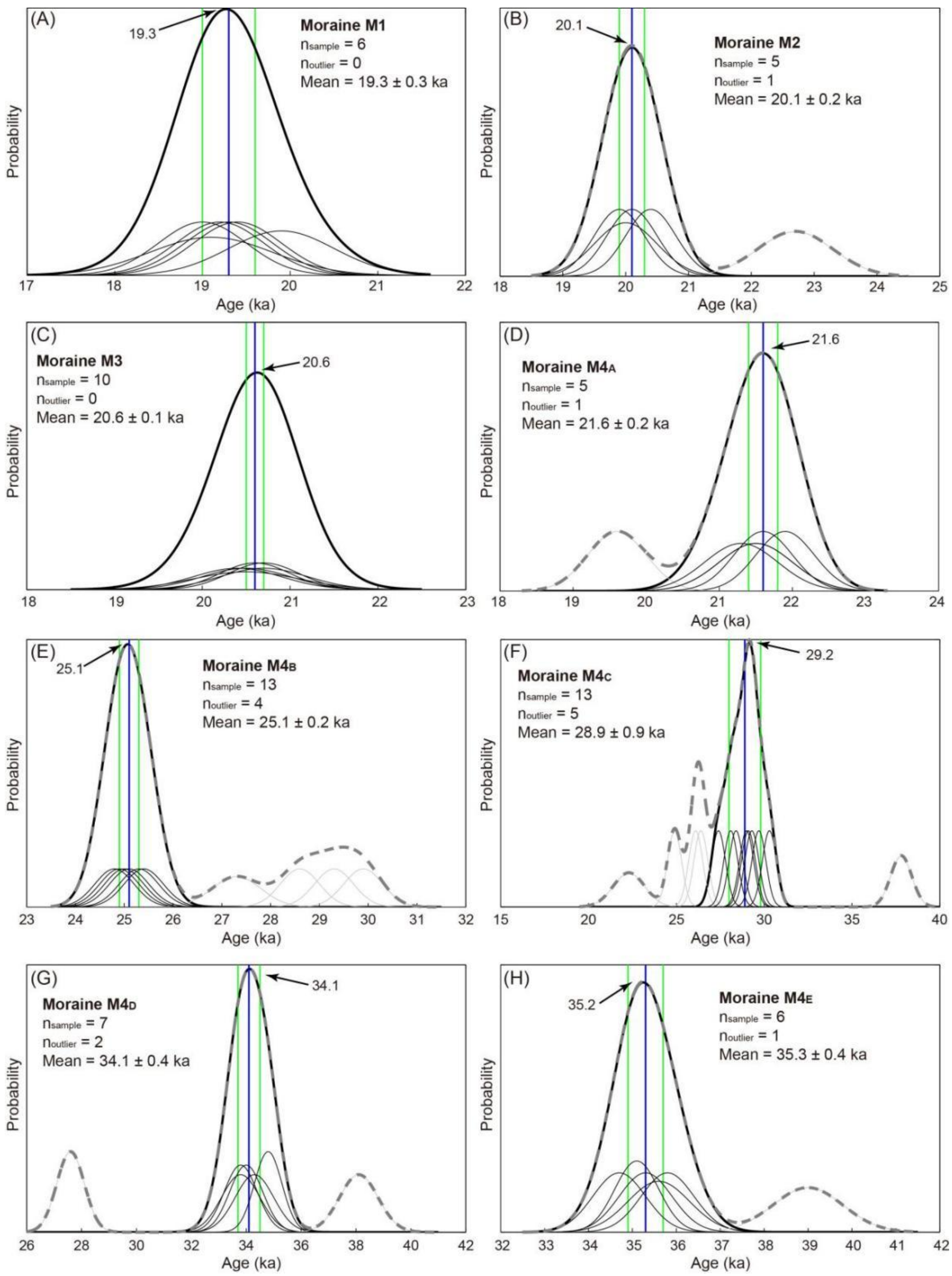

Supplementary Figure 2 Probability density function (PDF) and summary statistics for ^{10}Be ages from the M1 (A), M2 (B), M3 (C), and M4 (D-H) moraines. The thin curves are individual sample PDFs defined by ^{10}Be ages and their 1σ analytical uncertainties, with the light grey indicating potential outliers identified by the 1σ-level approach. The thick dark grey dashed lines represent a cumulative PDF for an age group with outliers included. The thick black curves denote a cumulative PDF of outlier-free subset. The blue vertical lines delineate the arithmetic mean of outlier-free population, while the green vertical lines illustrate the ±1σ standard deviation. Peak ages for each group are displayed by black arrows.

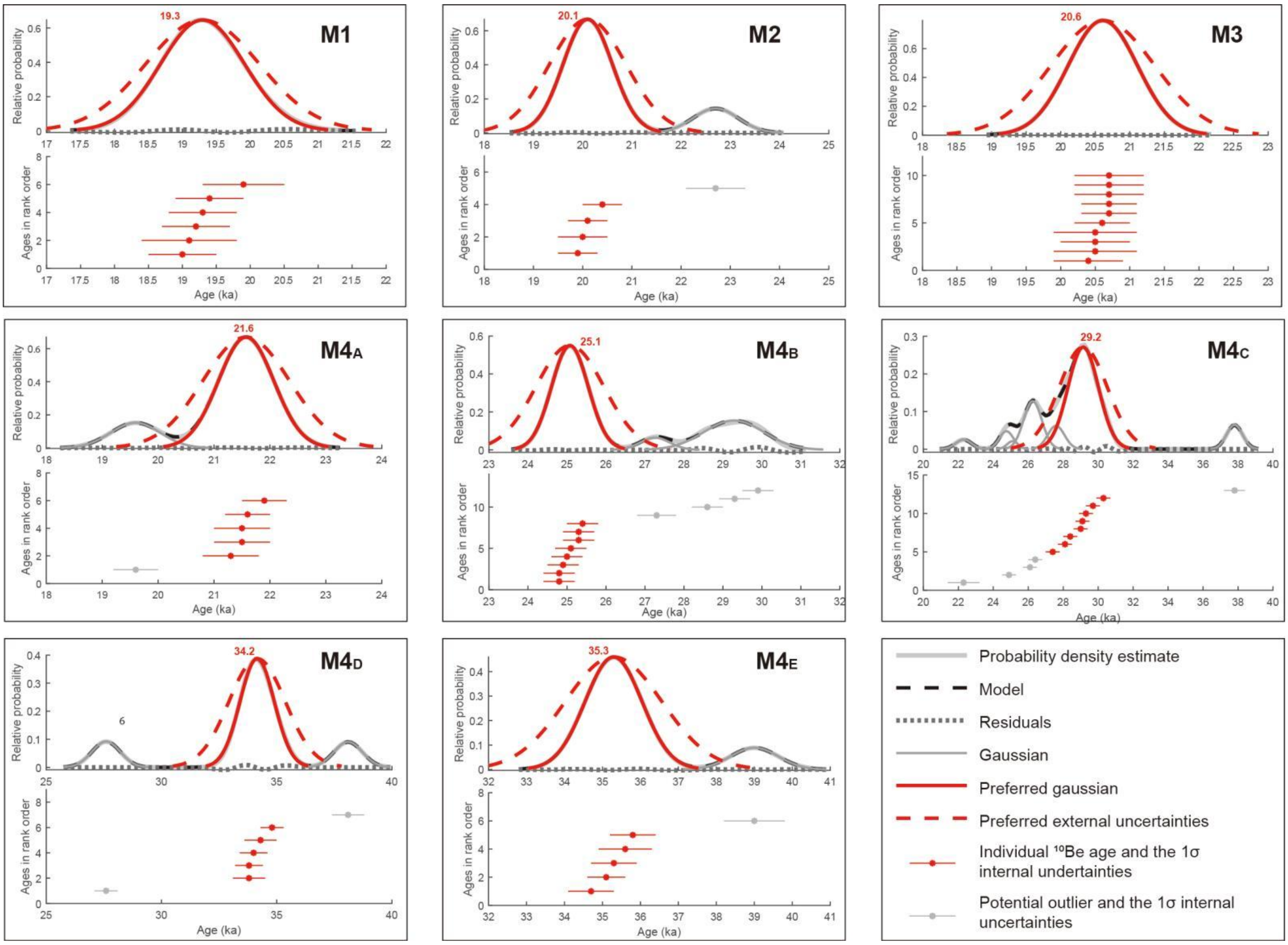

Supplementary Figure 3 Outlier detection results obtained using the P-CAAT program, developed by Dortch et al.[26].

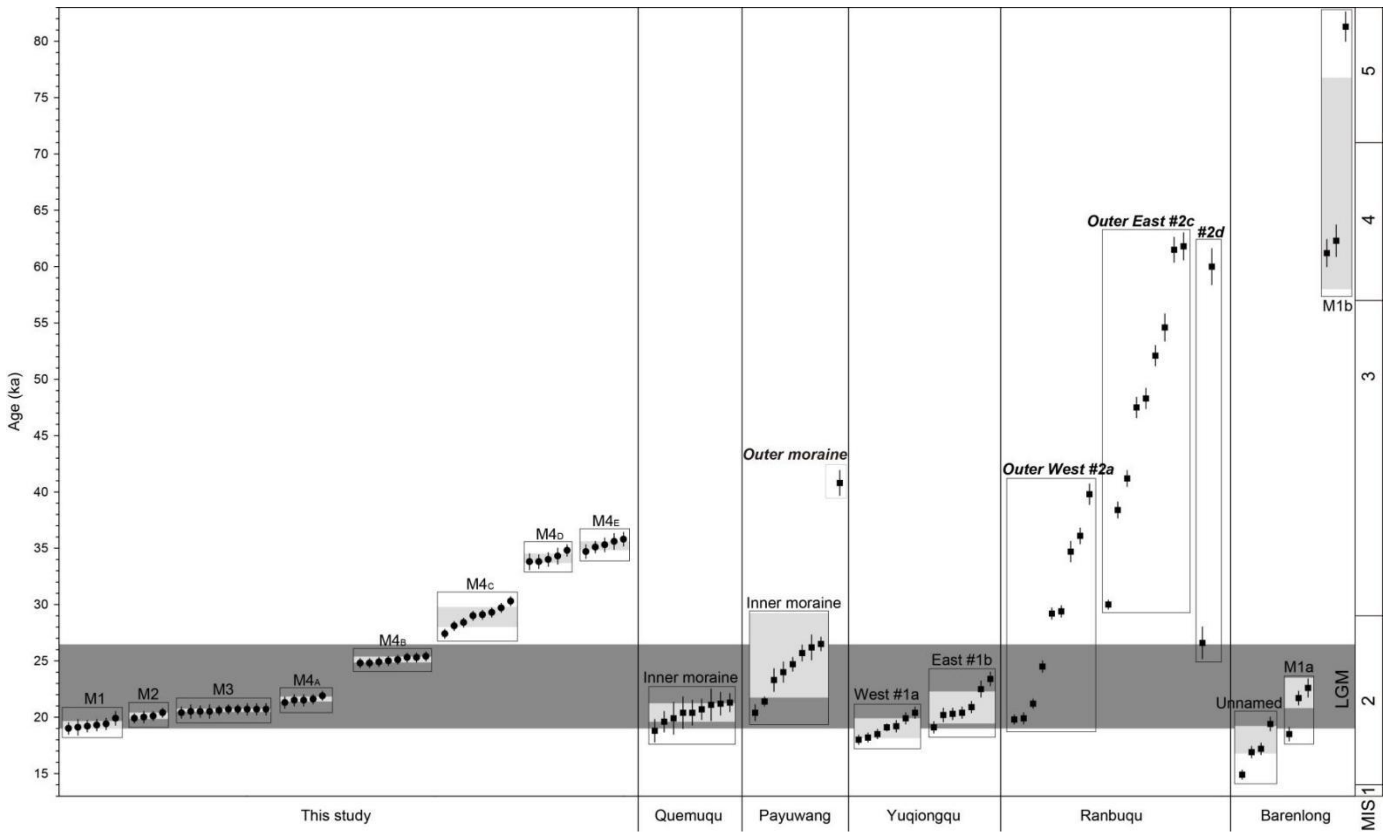

Supplementary Figure 4 Comparison of the last glacial moraine chronologies between valleys across the western Nyainqentanglha Mountains. Exposure-ages from each valley are plotted from youngest to oldest, with their 1σ internal uncertainties, against the relative position of moraines in each valley. Individual ^{10}Be ages are illustrated by black dots and rectangles for the studied Sibuqu Valley and other valleys (Fig. 1), respectively. Black boxes surround ^{10}Be data that are obtained from the same moraine. Given above and below the boxes are moraine names, with the italic bold denoting the poorly-dated (Class C; see also Supplementary Table 4) moraines that are not included in comparison of moraine chronologies. Shown in the right-most panel are Marine Isotope Stages 1–5 (MIS 1–5)[14]. The horizontal dark grey band represents the Last Glacial Maximum (LGM)[15] time.

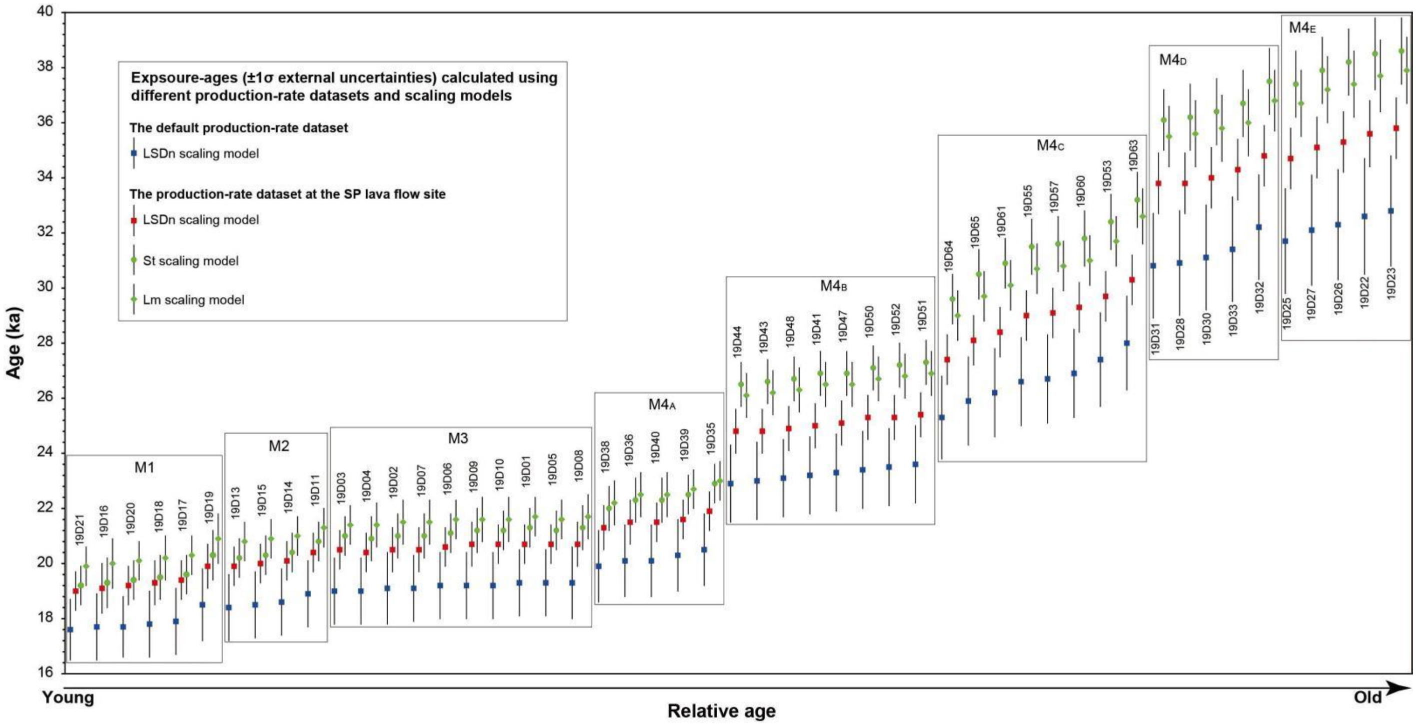

Supplementary Figure 5 Plots of outlier-free ^{10}Be data obtained using different production-rate datasets[34–36] and scaling models[30–33], from youngest to oldest, for each individual moraine in the Sibuqu Valley.

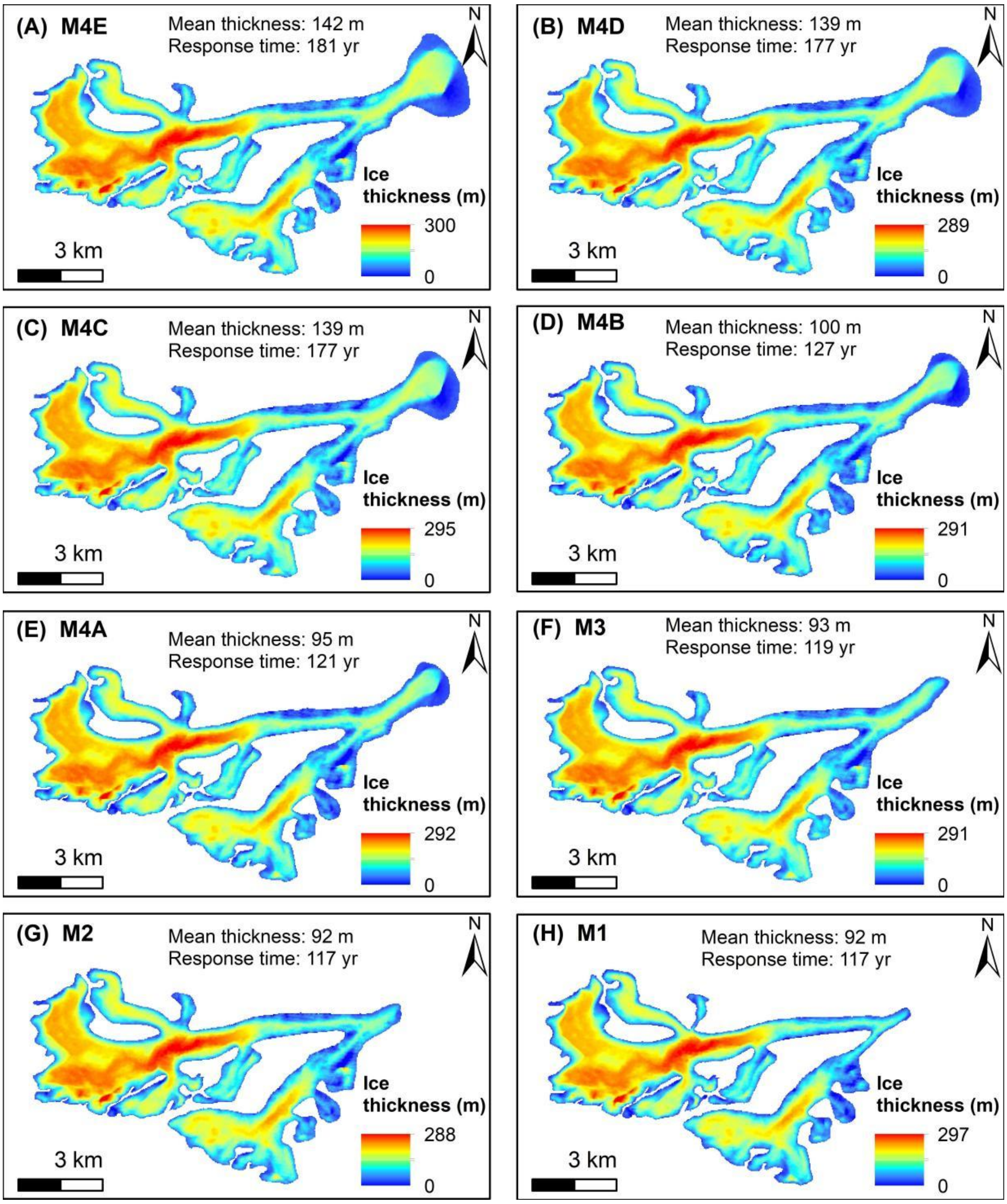

Supplementary Figure 6 Ice thickness reconstructed for the identified millennial-scale glacial culminations using a python-based tool[40] and corresponding response time of glaciers that was estimated based on the method developed by Jóhannesson et al.[39].

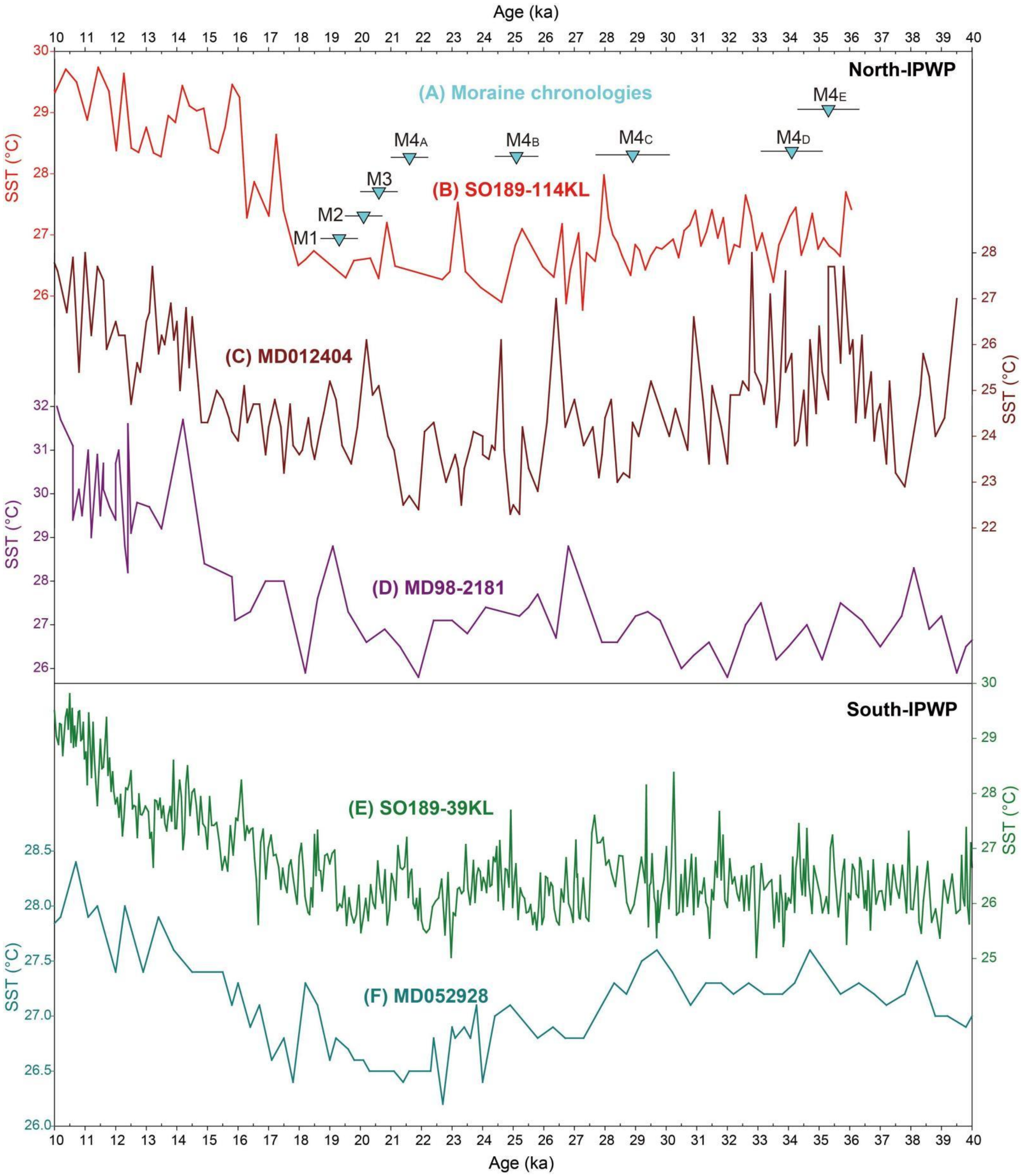

Supplementary Figure 7 Comparision between moraine chronologies (A) and the reconstructed SSTs in the north-IPWP (B–D)[43–45] and south-IPWP (E and F)[43, 46].

Supplementary Table 1 Details of boulder samples and results of ^{10}Be surface exposure dating in the Sibuqu Valley, the western-most segment of WNM, southern TP.

Sample ID[a]	Latitude (°N)	Longitude (°E)	Elevation (m asl)	Boulder size (L/W/H) (cm)	Sample thickness (cm)	Shielding correction[b]	Quartz weight (g)	Carrier weight (g)[c]	^{10}Be/^{9}Be (10^{-15})[d]	^{10}Be concentration (atoms/g)[e]	Exposure-age (ka)		
											LSDn scaling model[30]	St scaling model[31, 32]	Lm scaling model[31–33]
						Moraine M1 (n = 6; class A)[f]							
19D16	29.79822	90.29634	4703	276/231/165	1.7	0.9919	30.9908	0.3112	1688.69 ± 57.19	1110211 ± 39334	19.1 ± 0.7 (0.9)	19.3 ± 0.7 (0.9)	20.0 ± 0.7 (0.9)
19D17	29.79813	90.29631	4706	131/125/51	1.0	0.9913	29.6832	0.3153	1636.45 ± 36.25	1138006 ± 27776	19.4 ± 0.5 (0.7)	19.6 ± 0.5 (0.7)	20.3 ± 0.5 (0.7)
19D18	29.79807	90.29622	4706	107/89/52	1.5	0.9913	29.5829	0.3145	1617.83 ± 41.63	1125961 ± 31208	19.3 ± 0.5 (0.8)	19.5 ± 0.5 (0.8)	20.2 ± 0.6 (0.8)
19D19	29.79784	90.29595	4708	123/92/65	0.9	0.9912	18.5519	0.3146	1061.95 ± 32.50	1177223 ± 38146	19.9 ± 0.6 (0.8)	20.3 ± 0.7 (0.9)	20.9 ± 0.7 (0.9)
19D20	29.79825	90.29598	4703	313/300/143	3.2	0.9916	29.3115	0.3136	1572.27 ± 37.18	1101132 ± 28393	19.2 ± 0.5 (0.7)	19.4 ± 0.5 (0.7)	20.1 ± 0.5 (0.7)
19D21	29.79796	90.29603	4706	141/105/72	1.3	0.9912	30.1292	0.3175	1606.50 ± 38.92	1108286 ± 29165	19.0 ± 0.5 (0.7)	19.2 ± 0.5 (0.7)	19.9 ± 0.5 (0.7)
						Moraine M2 (n =5; class A)[f]							
19D11	29.79965	90.29782	4691	96/83/61	0.5	0.9961	29.8340	0.3153	1748.19 ± 33.25	1209776 ± 26109	20.4 ± 0.4 (0.7)	20.8 ± 0.5 (0.7)	21.3 ± 0.5 (0.7)
19D12	29.79928	90.29741	4686	89/67/53	2.0	0.9908	30.4345	0.3179	2002.60 ± 45.36	1370155 ± 34030	22.7 ± 0.6 (0.8)	24.1 ± 0.6 (0.9)	24.1 ± 0.6 (0.9)
19D13	29.79923	90.29704	4686	78/61/55	3.7	0.9906	30.1828	0.3168	1646.17 ± 32.38	1131204 ± 25073	19.9 ± 0.4 (0.7)	20.2 ± 0.4 (0.7)	20.8 ± 0.5 (0.7)
19D14	29.79882	90.29723	4690	190/133/72	2.4	0.9871	30.3994	0.3149	1706.18 ± 32.28	1157198 ± 24876	20.1 ± 0.4 (0.7)	20.4 ± 0.4 (0.7)	21.0 ± 0.5 (0.7)
19D15	29.79929	90.29705	4687	97/81/54	4.6	0.9906	30.2479	0.3140	1666.51 ± 33.44	1132629 ± 25503	20.0 ± 0.5 (0.7)	20.3 ± 0.5 (0.7)	20.9 ± 0.5 (0.7)
						Moraine M3 (n = 10; class A)[f]							
19D01	29.79932	90.30311	4670	82/62/55	1.0	0.9918	29.8159	0.3164	1743.09 ± 29.10	1212875 ± 23645	20.7 ± 0.4 (0.7)	21.3 ± 0.4 (0.7)	21.7 ± 0.4 (0.7)
19D02	29.79871	90.30246	4673	70/43/25	3.8	0.9951	29.9700	0.3164	1696.67 ± 45.61	1174465 ± 33733	20.5 ± 0.6 (0.8)	21.0 ± 0.6 (0.8)	21.5 ± 0.6 (0.8)
19D03	29.79861	90.30206	4678	166/61/68	6.1	0.9953	30.0021	0.3165	1667.34 ± 33.30	1153268 ± 25801	20.5 ± 0.5 (0.7)	21.0 ± 0.5 (0.7)	21.4 ± 0.5 (0.7)
19D04	29.79860	90.30211	4678	138/55/50	5.9	0.9953	29.8582	0.3171	1653.14 ± 35.69	1151129 ± 27437	20.4 ± 0.5 (0.7)	20.9 ± 0.5 (0.8)	21.4 ± 0.5 (0.8)
19D05	29.79827	90.30162	4684	85/66/35	5.5	0.9944	31.1691	0.3164	1768.14 ± 29.39	1176907 ± 22869	20.7 ± 0.4 (0.7)	21.2 ± 0.4 (0.7)	21.6 ± 0.4 (0.7)
19D06	29.80024	90.30051	4657	88/65/28	3.7	0.9922	30.4986	0.3162	1722.82 ± 27.56	1171174 ± 22133	20.6 ± 0.4 (0.7)	21.1 ± 0.4 (0.7)	21.6 ± 0.4 (0.7)
19D07	29.80074	90.30072	4652	53/39/15	5.9	0.9929	30.0814	0.3128	1673.76 ± 42.16	1141147 ± 30977	20.5 ± 0.6 (0.8)	21.0 ± 0.6 (0.8)	21.5 ± 0.6 (0.8)
19D08	29.80086	90.30081	4653	148/117/37	3.1	0.9936	29.7389	0.3144	1707.08 ± 41.24	1183324 ± 30988	20.7 ± 0.5 (0.8)	21.3 ± 0.6 (0.8)	21.7 ± 0.6 (0.8)
19D09	29.80074	90.30089	4657	75/65/45	4.9	0.9930	29.6015	0.3131	1678.34 ± 40.58	1163943 ± 30502	20.7 ± 0.5 (0.8)	21.2 ± 0.6 (0.8)	21.6 ± 0.6 (0.8)
19D10	29.80133	90.30125	4647	53/44/25	4.0	0.9936	30.2170	0.3156	1701.52 ± 33.92	1165241 ± 26034	20.7 ± 0.5 (0.7)	21.2 ± 0.5 (0.7)	21.6 ± 0.5 (0.8)

Moraine $M4_{A}$ (n = 6; class A)[f]													
19D35	29.80522	90.31394	4516	143/121/96	3.1	0.9964	30.4037	0.3226	1720.00 ± 23.10	1196625 ± 20077	21.9 ± 0.4 (0.7)	22.9 ± 0.4 (0.7)	23.0 ± 0.4 (0.7)
19D36	29.80501	90.31392	4517	109/102/75	4.9	0.9962	29.8664	0.3174	1650.00 ± 34.10	1149659 ± 26441	21.5 ± 0.5 (0.8)	22.3 ± 0.5 (0.8)	22.5 ± 0.5 (0.8)
19D37	29.80425	90.31393	4518	240/175/97	1.5	0.9954	30.3826	0.3121	1560.00 ± 29.70	1050542 ± 22637	19.6 ± 0.4 (0.7)	19.8 ± 0.4 (0.7)	20.4 ± 0.4 (0.7)
19D38	29.80391	90.31398	4519	232/202/195	5.7	0.9955	29.0712	0.3283	1520.00 ± 34.50	1125345 ± 27961	21.3 ± 0.5 (0.8)	22.0 ± 0.5 (0.8)	22.2 ± 0.6 (0.8)
19D39	29.80289	90.31351	4521	273/161/59	4.6	0.9957	29.9278	0.3259	1630.00 ± 24.20	1163767 ± 20874	21.6 ± 0.4 (0.7)	22.5 ± 0.4 (0.7)	22.7 ± 0.4 (0.7)
19D40	29.80313	90.31366	4519	175/145/102	5.2	0.9959	29.7845	0.3242	1610.00 ± 29.30	1148968 ± 23903	21.5 ± 0.5 (0.7)	22.3 ± 0.5 (0.8)	22.5 ± 0.5 (0.8)
Moraine $M4_{B}$ (n = 12; class A)[f]													
19D41	29.80065	90.31499	4526	160/140/100	1.1	0.9956	30.9746	0.3233	2092.79 ± 26.29	1432396 ± 23028	25.0 ± 0.4 (0.8)	26.9 ± 0.4 (0.8)	26.5 ± 0.4 (0.8)
19D42	29.80011	90.31464	4525	169/92/85	3.9	0.9959	30.4835	0.3191	2417.47 ± 26.17	1659654 ± 24488	29.3 ± 0.4 (0.9)	31.9 ± 0.5 (1.0)	31.1 ± 0.5 (1.0)
19D43	29.80090	90.31522	4525	70/55/50	4.5	0.9956	30.3496	0.3205	1987.25 ± 23.44	1376057 ± 21310	24.8 ± 0.4 (0.8)	26.6 ± 0.4 (0.8)	26.2 ± 0.4 (0.8)
19D44	29.80147	90.31550	4521	156/81/60	1.7	0.9955	30.1894	0.3198	2017.67 ± 20.96	1401490 ± 20238	24.8 ± 0.4 (0.8)	26.5 ± 0.4 (0.8)	26.1 ± 0.4 (0.8)
19D45	29.80168	93.31448	4524	143/79/34	4.4	0.9955	31.2434	0.3218	2254.06 ± 29.43	1522517 ± 25069	27.3 ± 0.5 (0.9)	29.5 ± 0.5 (0.9)	28.9 ± 0.5 (0.9)
19D46	29.80111	90.31536	4521	202/166/68	6.3	0.9956	29.9660	0.3198	2376.11 ± 21.60	1663050 ± 22503	29.9 ± 0.4 (0.9)	32.7 ± 0.4 (1.0)	32.0 ± 0.4 (1.0)
19D47	29.80431	90.31549	4506	79/94/77	4.0	0.9957	29.8178	0.3216	1960.97 ± 23.23	1386805 ± 21528	25.1 ± 0.4 (0.8)	26.9 ± 0.4 (0.8)	26.5 ± 0.4 (0.8)
19D48	29.80429	90.31546	4503	89/53/26	1.9	0.9955	31.4344	0.3224	2077.50 ± 22.12	1397220 ± 20436	24.9 ± 0.4 (0.8)	26.7 ± 0.4 (0.8)	26.3 ± 0.4 (0.8)
19D49	29.80411	90.31552	4505	90/67/48	5.7	0.9957	32.3556	0.3189	2441.61 ± 26.86	1578266 ± 23493	28.6 ± 0.4 (0.9)	31.1 ± 0.5 (1.0)	30.3 ± 0.5 (0.9)
19D50	29.80368	90.31567	4504	234/139/143	3.8	0.9957	29.6709	0.3197	1980.68 ± 18.81	1399370 ± 19327	25.3 ± 0.4 (0.8)	27.1 ± 0.4 (0.8)	26.7 ± 0.4 (0.8)
19D51	29.80370	90.31564	4509	81/77/49	1.8	0.9960	31.2181	0.3229	2115.39 ± 22.62	1434810 ± 21034	25.4 ± 0.4 (0.8)	27.3 ± 0.4 (0.8)	26.9 ± 0.4 (0.8)
19D52	29.80310	90.31564	4504	115/70/53	1.1	0.9954	31.4926	0.3201	2154.24 ± 21.36	1435878 ± 20248	25.3 ± 0.4 (0.8)	27.2 ± 0.4 (0.8)	26.8 ± 0.4 (0.8)
Moraine $M4_{C}$ (n = 13; class B)[f]													
19D53	29.80266	90.31693	4497	113/98/59	0.6	0.9952	29.7295	0.3198	2420.82 ± 20.26	1705985 ± 22307	29.7 ± 0.4 (0.9)	32.4 ± 0.4 (1.0)	31.7 ± 0.4 (0.9)
19D54	29.80290	90.31699	4498	86/74/44	0.6	0.9952	31.5718	0.3209	1866.81 ± 73.56	1242322 ± 50641	22.3 ± 0.9 (1.1)	23.5 ± 1.0 (1.2)	23.6 ± 1.0 (1.2)
19D55	29.80306	90.31701	4498	105/94/54	0.7	0.9955	30.6096	0.3190	2431.66 ± 25.06	1660200 ± 23904	29.0 ± 0.4 (0.9)	31.5 ± 0.5 (1.0)	30.7 ± 0.4 (0.9)
19D56	29.80335	90.31705	4497	177/137/59	1.0	0.9955	31.4983	0.3222	2206.57 ± 20.66	1478429 ± 20312	26.1 ± 0.4 (0.8)	28.1 ± 0.4 (0.8)	27.6 ± 0.4 (0.8)
19D57	29.80355	90.31705	4498	90/80/40	0.6	0.9957	30.5788	0.3207	2429.22 ± 24.79	1669066 ± 23911	29.1 ± 0.4 (0.9)	31.6 ± 0.5 (1.0)	30.8 ± 0.4 (0.9)
19D58	29.80381	90.31704	4498	118/112/84	1.1	0.9959	30.9038	0.3223	2052.33 ± 23.33	1401741 ± 21287	24.9 ± 0.4 (0.8)	26.6 ± 0.4 (0.8)	26.3 ± 0.4 (0.8)
19D59	29.80400	90.31711	4498	211/184/84	2.4	0.9959	30.8939	0.3220	2173.80 ± 20.34	1486392 ± 20372	26.4 ± 0.4 (0.8)	28.6 ± 0.4 (0.9)	28.0 ± 0.4 (0.8)
19D60	29.80411	90.31699	4497	141/111/61	0.7	0.9962	30.4531	0.3215	2420.66 ± 25.07	1676646 ± 24154	29.3 ± 0.4 (0.9)	31.8 ± 0.5 (1.0)	31.0 ± 0.5 (0.9)
19D61	29.80419	90.31707	4500	207/151/89	1.9	0.9962	30.2375	0.3234	2299.96 ± 21.19	1613843 ± 21958	28.4 ± 0.4 (0.9)	30.9 ± 0.4 (0.9)	30.1 ± 0.4 (0.9)
19D62	29.80430	90.31706	4499	160/79/17	0.8	0.9967	20.4728	0.3208	2091.50 ± 24.30	2149972 ± 32984	37.8 ± 0.6 (1.2)	40.8 ± 0.6 (1.3)	39.6 ± 0.6 (1.2)
19D63	29.80443	90.31719	4499	86/84/45	0.9	0.9966	30.1624	0.3173	2532.39 ± 23.22	1747835 ± 23730	30.3 ± 0.4 (0.9)	33.2 ± 0.5 (1.0)	32.6 ± 0.4 (1.0)

19D64	29.80467	90.31719	4497	111/70/41	6.6	0.9966	30.1403	0.3225	2123.40 ± 23.39	1490517 ± 22194	27.4 ± 0.4 (0.9)	29.6 ± 0.4 (0.9)	29.0 ± 0.4 (0.9)
19D65	29.80459	90.31716	4497	80/65/35	5.0	0.9966	29.7126	0.3218	2183.23 ± 21.06	1551226 ± 21572	28.1 ± 0.4 (0.9)	30.5 ± 0.4 (0.9)	29.7 ± 0.4 (0.9)
Moraine $M4_D$ (n = 7; class A)[f]													
19D28	29.80577	90.31910	4490	135/121/79	4.8	0.9966	30.2738	0.3134	2706.93 ± 45.96	1838343 ± 36255	33.8 ± 0.7 (1.1)	36.2 ± 0.7 (1.2)	35.6 ± 0.7 (1.2)
19D29	29.80581	90.31913	4490	208/152/109	2.7	0.9966	30.4303	0.3164	2263.24 ± 32.54	1543566 ± 27068	27.6 ± 0.5 (0.9)	29.8 ± 0.5 (1.0)	29.2 ± 0.5 (0.9)
19D30	29.86532	90.31914	4491	181/145/125	2.8	0.9963	30.0018	0.3145	2735.81 ± 43.60	1881398 ± 35434	34.0 ± 0.6 (1.1)	36.4 ± 0.7 (1.2)	35.8 ± 0.7 (1.2)
19D31	29.80522	90.31910	4492	121/109/75	2.2	0.9963	30.0237	0.3144	2730.00 ± 36.50	1875228 ± 31344	33.8 ± 0.6 (1.1)	36.1 ± 0.6 (1.1)	35.5 ± 0.6 (1.1)
19D32	29.80468	90.31924	4494	98/85/73	0.6	0.9965	30.0770	0.3136	2890.00 ± 30.70	1976651 ± 28870	34.8 ± 0.5 (1.1)	37.5 ± 0.6 (1.2)	36.8 ± 0.5 (1.1)
19D33	29.80098	90.31922	4494	84/71/60	1.5	0.9480	30.4830	0.3152	2690.00 ± 43.10	1824525 ± 34496	34.3 ± 0.7 (1.1)	36.7 ± 0.7 (1.2)	36.0 ± 0.7 (1.2)
19D34	29.80097	90.31920	4494	74/63/49	4.3	0.9480	30.1878	0.3099	2970.00 ± 47.00	2000055 ± 37476	38.1 ± 0.7 (1.3)	41.2 ± 0.8 (1.4)	39.9 ± 0.8 (1.3)
Moraine $M4_E$ (n = 6; class A)[f]													
19D22	29.80186	90.32004	4487	155/121/97	1.2	0.9795	30.2785	0.3160	2882.59 ± 51.81	1973664 ± 40630	35.6 ± 0.7 (1.2)	38.5 ± 0.8 (1.3)	37.7 ± 0.8 (1.3)
19D23	29.80271	90.31998	4487	181/131/112	2.0	0.9781	29.9180	0.3152	2845.02 ± 36.95	1966401 ± 32266	35.8 ± 0.6 (1.1)	38.6 ± 0.6 (1.2)	37.9 ± 0.6 (1.2)
19D24	29.80299	90.32007	4488	195/144/132	2.9	0.9874	30.3176	0.3152	3164.20 ± 51.72	2158317 ± 41389	39.0 ± 0.8 (1.3)	42.3 ± 0.8 (1.4)	40.7 ± 0.8 (1.3)
19D25	29.80300	90.32007	4489	320/250/213	5.7	0.9874	30.4173	0.3054	2831.76 ± 38.55	1865214 ± 31538	34.7 ± 0.6 (1.1)	37.4 ± 0.6 (1.2)	36.7 ± 0.6 (1.2)
19D26	29.80304	90.32004	4490	75/62/47	4.7	0.9914	30.2088	0.3166	2805.71 ± 35.18	1929079 ± 30971	35.3 ± 0.6 (1.1)	38.2 ± 0.6 (1.2)	37.4 ± 0.6 (1.2)
19D27	29.80457	90.31968	4491	62/53/41	4.9	0.9965	30.6431	0.3151	2853.21 ± 33.79	1924788 ± 29865	35.1 ± 0.5 (1.1)	37.9 ± 0.6 (1.2)	37.2 ± 0.6 (1.2)

Notation: All boulder samples were processed at the Xi'an-AMS Center, Institute of Earth Environment, CAS. Beryllium ratios were measured at the center against the ICN 1-05-4 standardization[49], with an assigned $^{10}Be/^{9}Be$ ratio of 2.851×10^{-12}. Exposure-ages were calculated using the CRONUS online calculator[33] (version 3) with the dataset of ^{10}Be production-rates calibrated by Fenton et al.[34, 35] at the SP lava flow calibration site, North America.

[a] Bold italics indicate potential outliers found by the 1σ-level statistics.

[b] Shielding factors are determined by using the python tool developed by Li[39].

[c] Beryllium carrier used in this study has a concentration of 982.37 ppm.

[d] Isotopic ratios are reported here without blank correction.

[e] The released ^{10}Be concentrations are blank-corrected using seven blanks with values of $(2.01 \pm 1.20) \times 10^{-15}$ (for samples 19D01–19D10), $(4.55 \pm 2.27) \times 10^{-15}$ (for 19D11–19D21),

(1.78 ± 1.26) × 10^{-15} (for 19D22–19D30), (2.16 ± 1.25) × 10^{-15} (for 19D31–19D40), (2.27 ± 0.72) × 10^{-15} (for 19D41–19D52), (4.87 ± 1.17) × 10^{-15} (for 19D53–19D58), and (1.38 ± 0.53) × 10^{-15} (for 19D59–19D65).

[f] Moraines were divided into class A (well-clustered), B (moderately-clustered), and C (poorly-clustered) qualities following Blomdin et al. [28, 29].

Supplementary Table 2 Outlier statistics using the Pierce's criterion approach[27]. The detected potential outliers are denoted by italic bold.

Moraine name	Sample ID	^{10}Be age (ka)	Mean of all ages (ka)	Standard deviation	R value (assumed number of outliers)	Maximum allowable deviation	Absolute value of mean minus individual age	Outlier? (Y/N)
M1	19D16	19.1	19.32	0.32	1.610 (1)	0.515	0.220	N
	19D17	19.4			1.299 (2)	0.416	0.080	N
	19D18	19.3					0.020	N
	19D19	19.9					0.580	Y
	19D20	19.2					0.120	N
	19D21	19.0					0.320	N
M2	19D11	20.4	20.62	1.18	1.509 (1)	1.781	0.220	N
	19D12	22.7			1.200 (2)	1.416	2.080	Y
	19D13	19.9					0.720	N
	19D14	20.1					0.520	N
	19D15	20.0					0.620	N
M3	19D01	20.7	20.60	0.12	1.878 (1)	0.225	0.100	N
	19D02	20.5					0.100	N
	19D03	20.5					0.100	N
	19D04	20.4					0.200	N
	19D05	20.7					0.100	N
	19D06	20.6					0.000	N
	19D07	20.5					0.100	N
	19D08	20.7					0.100	N
	19D09	20.7					0.100	N
	19D10	20.7					0.100	N
$M4_A$	19D35	21.9	21.23	0.82	1.610 (1)	1.320	0.67	N
	19D36	21.5			1.299 (2)	1.065	0.27	N
	19D37	19.6					1.63	Y
	19D38	21.3					0.07	N
	19D39	21.6					0.37	N
	19D40	21.5					0.27	N
$M4_B$	19D41	25.0	26.31	1.92	1.969 (1)	3.780	1.31	N
	19D42	29.3					2.99	N
	19D43	24.8					1.51	N
	19D44	24.8					1.51	N
	19D45	27.3					0.99	N

	19D46	29.9					3.59	N
	19D47	25.1					1.21	N
	19D48	24.9					1.41	N
	19D49	28.6					2.29	N
	19D50	25.3					1.01	N
	19D51	25.4					0.91	N
	19D52	25.3					1.01	N
	19D53	29.7			2.007 (1)	7.225	1.33	N
	19D54	22.3			1.704 (2)	6.134	6.07	N
	19D55	29.0					0.63	N
	19D56	26.1					2.27	N
	19D57	29.1					0.73	N
	19D58	24.9					3.47	N
$M4_C$	19D59	26.4	28.37	3.6			1.97	N
	19D60	29.3					0.93	N
	19D61	28.4					0.03	N
	19D62	37.8					9.43	Y
	19D63	30.3					1.93	N
	19D64	27.4					0.97	N
	19D65	28.1					0.27	N
	19D28	33.8			1.693 (1)	5.265	0.03	N
	19D29	27.6			1.382 (2)	4.298	6.17	Y
	19D30	34.0			1.187 (3)	3.692	0.23	N
$M4_D$	19D31	33.8	33.77	3.11			0.03	N
	19D32	34.8					1.03	N
	19D33	34.3					0.53	N
	19D34	38.1					4.33	Y
	19D22	35.6			1.610 (1)	2.512	0.32	N
	19D23	35.8			1.299 (2)	2.026	0.12	N
	19D24	39.0					3.08	Y
$M4_E$	19D25	34.7	35.92	1.56			1.22	N
	19D26	35.3					0.62	N
	19D27	35.1					0.82	N

Supplementary Table 3 Comparison of outlier detection results between the '1σ-level' method and other two widely-used approaches (P-CAAT[26] and Pierce's criterion[27]). More details about results given by these two approaches can be found in Supplementary Fig. 3 and Table 2.

Moraine name	Outlier detection results					
	This study		P-CAAT[26]		Pierce's criterion[27]	
	Number of outliers	Identified outlier (s)	Number of outliers	Identified outlier (s)	Number of outliers	Identified outlier (s)
M1	1	19D19	1	19D19	1	19D19
M2	1	19D12	1	19D12	1	19D12
M3	0	-	0	-	0	-
$M4_A$	1	19D37	1	19D37	1	19D37
$M4_B$	4	19D42, 45, 46, and 49	4	19D42, 45, 46, and 49	0	-
$M4_C$	5	19D54, 56, 58, 59, and 62	5	19D54, 56, 58, 59, and 62	1	19D62
$M4_D$	2	19D29 and 34	2	19D29 and 34	2	19D29 and 34
$M4_E$	1	19D24	1	19D24	1	19D24

Supplementary Table 4 Updated ^{10}Be exposure-ages and related information used to recalculate exposure-ages across the WNM, southern TP. Exposure-ages were recalculated using the CRONUS online calculator[33] (version 3) with the dataset of ^{10}Be production-rates calibrated by Fenton et al.[34, 35] at the SP lava flow calibration site, North America.

Source	Valley name	Site No. in Fig. 1	Moraine name and classification	Sample ID[a]	Latitude (°N)	Longitude (°E)	Elevation (m asl)	Elevation flag	Sample thickness (cm)	Density (g/cm^3)	Shielding correction	^{10}Be concentration (atoms/g)	Error in ^{10}Be concentration (atoms/g)	^{10}Be standard	Exposure-age (ka)[b]
Dong et al. [17]	Quemuqu Valley	2	Inner moraine (class A)[c]	NQDGL15-01	29.90056	90.06389	4984	std	2.5	2.7	0.9966	1435800	94700	07KNSTD	21.1 + 1.4 (1.5)
				NQDGL15-02	29.85053	90.06394	4980	std	4.5	2.7	0.9966	126100	13700	07KNSTD	2.5 + 0.3 (0.3)
				NQDGL15-05	29.85169	90.06444	4982	std	4.5	2.7	0.9966	1306900	90200	07KNSTD	19.9 + 1.4 (1.5)
				NQDGL15-06	29.85097	90.06469	4997	std	5	2.7	0.9966	1224000	66200	07KNSTD	18.8 + 1.0 (1.1)
				NQDGL15-07	29.85039	90.06444	4970	std	4.5	2.7	0.9966	1342900	93500	07KNSTD	20.4 + 1.4 (1.5)
				NQDGL15-08	29.84264	90.06400	4899	std	4.5	2.7	0.9966	1236900	55400	07KNSTD	19.6 + 0.9 (1.0)
				NQDGL15-09	29.84244	90.06403	4872	std	4.5	2.7	0.9966	1276400	68100	07KNSTD	20.4 + 1.1 (1.2)
				NQDGL15-10	29.84256	90.06386	4864	std	4.5	2.7	0.9966	1346800	47500	07KNSTD	21.3 + 0.8 (1.0)
				NQDGL15-11	29.84258	90.06383	4858	std	4.4	2.7	0.9966	1341200	59900	07KNSTD	21.2 + 1.0 (1.1)
				NQDGL15-12	29.84244	90.06361	4848	std	5	2.7	0.9966	1285000	52800	07KNSTD	20.7 + 0.9 (1.0)
Dong et al. [18]	Payuwang Valley	5	Inner moraine (class B)[c]	Nam-51	30.59839	90.77305	4952	std	3	2.7	0.9929	1690000	60000	07KNSTD	24.0 + 0.9 (1.1)
				Nam-52	30.59849	90.77305	4953	std	3	2.7	0.9929	1370000	50000	07KNSTD	20.4 + 0.7 (0.9)
				Nam-53	30.59868	90.7727	4953	std	3	2.7	0.9929	1830000	50000	07KNSTD	25.7 + 0.7 (1.0)
				Nam-54	30.59871	90.77269	4953	std	3	2.7	0.9929	1870000	80000	07KNSTD	26.2 + 1.1 (1.3)
				Nam-55	30.59883	90.77251	4953	std	3	2.7	0.9929	1460000	30000	07KNSTD	21.4 + 0.4 (0.7)
				Nam-56	30.60160	90.77064	4927	std	2.5	2.7	0.9918	1880000	40000	07KNSTD	26.5 + 0.6 (0.9)
				Nam-57	30.60162	90.77064	4927	std	2.5	2.7	0.9918	2290000	50000	07KNSTD	32.4 + 0.7 (1.1)
				Nam-58	30.60189	90.7707	4925	std	2.5	2.7	0.9918	1730000	40000	07KNSTD	24.7 + 0.6 (0.9)
				Nam-59	30.60199	90.77067	4925	std	2.5	2.7	0.9918	1620000	70000	07KNSTD	23.3 + 1.0 (1.2)
				Nam-60	30.60198	90.77064	4925	std	2.5	2.7	0.9918	2190000	60000	07KNSTD	30.6 + 0.8 (1.2)
			Outer moraine (class C)[c]	***Nam-62***	30.61005	90.77416	4960	std	3	2.7	0.9977	1540000	70000	07KNSTD	22.0 + 1.0 (1.2)
				Nam-63	30.61002	90.77418	4960	std	3	2.7	0.9977	1380000	40000	07KNSTD	20.3 + 0.6 (0.8)
				Nam-64	30.61000	90.77417	4960	std	3	2.7	0.9977	2140000	160000	07KNSTD	29.5 + 2.2 (2.4)

				Nam-65	30.60966	90.77412	4960	std	3	2.7	0.9977	3030000	80000	07KNSTD	40.8 + 1.1 (1.6)
				Nam-66	30.60998	90.77413	4960	std	3	2.7	0.9977	1900000	80000	07KNSTD	26.3 + 1.1 (1.3)
Chevalier et al. [16]	Yuqiongqu Valley (**Gulu in the original publication**)	6	West #1a (class B)[c]	T5C-58	30.811	91.556	5003	std	4	2.7	0.991	1227000	24000	NIST_27900	18.2 + 0.4 (0.6)
				T5C-59	30.811	91.556	5003	std	4	2.7	0.991	1252000	24000	NIST_27900	18.5 + 0.4 (0.6)
				T5C-60	30.811	91.556	4995	std	4	2.7	0.995	1297000	23000	NIST_27900	19.1 + 0.3 (0.6)
				T5C-61	30.81	91.557	4988	std	4	2.7	0.995	1210000	25000	NIST_27900	18.0 + 0.4 (0.6)
				T5C-62	30.81	91.557	4991	std	4	2.7	0.995	1298000	37000	NIST_27900	19.2 + 0.5 (0.8)
				T5C-63	30.81	91.557	4991	std	4	2.7	0.995	1358000	34000	NIST_27900	19.9 + 0.5 (0.7)
				T5C-64	30.81	91.557	4987	std	4	2.7	0.994	1393000	35000	NIST_27900	20.4 + 0.5 (0.8)
			East #1b (class B)[c]	T5C-66	30.807	91.564	4874	std	4	2.7	0.997	1584000	40000	NIST_27900	23.4 + 0.6 (0.9)
				T5C-67	30.807	91.564	4874	std	4	2.7	0.997	1364000	34000	NIST_27900	20.9 + 0.5 (0.8)
				T5C-68	30.807	91.565	4858	std	4	2.7	0.997	1320000	35000	NIST_27900	20.4 + 0.5 (0.8)
				T5C-69	30.807	91.565	4840	std	4	2.7	0.997	1294000	32000	NIST_27900	20.3 + 0.5 (0.7)
				T5C-70	30.807	91.565	4860	std	4	2.7	0.997	1300000	40000	NIST_27900	20.2 + 0.6 (0.8)
				T5C-71	30.808	91.564	4876	std	4	2.7	0.996	1512000	47000	NIST_27900	22.5 + 0.7 (0.9)
				T5C-72	30.808	91.563	4869	std	4	2.7	0.996	1219000	30000	NIST_27900	19.1 + 0.5 (0.7)
	Rabuqu Valley (**Yanbajain in the original publication**)	4	Outer West #2a (class C)[c]	T5C-25	30.021	90.242	5276	std	4	2.7	0.982	2881000	52000	NIST_27900	19.9 + 0.5 (0.7)
				T5C-26	30.021	90.242	5258	std	4	2.7	0.982	2344000	42000	NIST_27900	36.1 + 0.7 (1.2)
				T5C-27	30.021	90.243	5248	std	4	2.7	0.982	1912000	37000	NIST_27900	29.4 + 0.5 (1.0)
				T5C-28	30.021	90.243	5227	std	4	2.7	0.986	2711000	70000	NIST_27900	24.5 + 0.5 (0.8)
				T5C-29	30.021	90.243	5221	std	4	2.7	0.999	3202000	74000	NIST_27900	34.7 + 0.9 (1.3)
				T5C-30	30.02	90.243	5206	std	4	2.7	0.999	4812000	103000	NIST_27900	39.8 + 0.9 (1.4)
				T5C-31	30.02	90.244	5200	std	4	2.7	0.999	1587000	30000	NIST_27900	62.0 + 1.3 (2.2)
				T5C-32	30.02	90.244	5200	std	4	2.7	0.999	1457000	26000	NIST_27900	21.2 + 0.4 (0.7)
				T5C-33	30.02	90.244	5184	std	4	2.7	0.999	2289000	41000	NIST_27900	19.8 + 0.4 (0.6)
				T5C-34	30.02	90.244	5177	std	4	2.7	0.999	2987000	53000	NIST_27900	29.2 + 0.5 (1.0)
			Outer East #2c (class C)[c]	T5C-35	30.018	90.248	5034	std	4	2.7	0.999	1485000	26000	NIST_27900	38.4 + 0.7 (1.3)
				T5C-36	30.018	90.248	5033	std	4	2.7	0.999	3903000	83000	NIST_27900	21.4 + 0.4 (0.7)
				T5C-37	30.018	90.247	5066	std	4	2.7	0.992	3624000	64000	NIST_27900	54.6 + 1.2 (1.9)
				T5C-38	30.018	90.248	5026	std	4	2.7	0.992	4350000	75000	NIST_27900	48.3 + 0.9 (1.6)
				T5C-39	30.018	90.248	5021	std	4	2.7	0.992	3081000	54000	07KNSTD	61.5 + 1.1 (2.0)

				T5C-40	30.018	90.248	5014	std	4	2.7	0.992	3504000	66000	NIST_27900	41.2 + 0.7 (1.3)
				T5C-41	30.018	90.249	5010	std	4	2.7	0.992	3719000	65000	NIST_27900	47.5 + 0.9 (1.6)
				T5C-42	30.017	90.249	4999	std	4	2.7	0.992	4321000	80000	07KNSTD	52.1 + 0.9 (1.7)
				T5C-43	30.017	90.249	4991	std	4	2.7	0.999	2163000	31000	07KNSTD	61.8 + 1.2 (2.1)
				T5C-44	30.017	90.249	4982	std	4	2.7	0.986	4112000	108000	NIST_27900	30.0 + 0.4 (0.9)
			#2d (class C)[c]	T5C-44bis	30.023	90.245	5239	std	4	2.7	0.986	2105000	113000	NIST_27900	60.0 + 1.6 (2.3)
				T5C-45	30.024	90.244	5261	std	4	2.7	0.986	1073000	32000	NIST_27900	26.6 + 1.4 (1.6)
Owen et al. [13]	Barenlong valley (**Gulu in the original publication**)	7	Unnamed (class B)[c]	PR48	30.78213333	91.52311667	4916	std	5	2.65	0.985	1440000	47900	LLNL3000	14.9 + 0.4 (0.6)
				PR49	30.78211667	91.52301667	4919	std	5	2.65	0.985	1260000	36600	LLNL3000	19.4 + 0.6 (0.8)
				PR50	30.78216667	91.52305000	4923	std	5	2.65	0.985	1240000	39900	LLNL3000	17.2 + 0.5 (0.7)
				PR51	30.78213333	91.52325000	4922	std	5	2.65	0.985	1370000	41700	LLNL3000	16.9 + 0.5 (0.7)
			M_{1a} (class A)[c]	PR52	30.77548333	91.54263333	4724	std	5	2.65	1	1630000	59700	LLNL3000	18.5 + 0.6 (0.8)
				PR53	30.77550000	91.54263333	4721	std	5	2.65	1	3537000	114000	LLNL3000	22.6 + 0.8 (1.0)
				PR54	30.77553333	91.54285000	4717	std	5	2.65	1	1540000	44500	LLNL3000	46.2 + 1.5 (2.0)
				PR55	30.77538333	91.54308333	4712	std	5	2.65	1	1480000	40800	LLNL3000	21.7 + 0.6 (0.9)
			M_{1b} (class B)[c]	***PR43***	30.77611667	91.59861667	4667	std	5	2.65	1	4310000	80400	LLNL3000	21.2 + 0.6 (0.8)
				PR44	30.77563333	91.59893333	4669	std	5	2.65	1	5800000	92900	LLNL3000	61.2 + 1.2 (2.0)
				PR45	30.77330000	91.59863333	4687	std	5	2.65	1	8980000	219000	LLNL3000	81.3 + 1.3 (2.6)
				PR46	30.77210000	91.59966667	4712	std	5	2.65	1	4510000	102000	LLNL3000	117.9 + 3.0 (4.4)
				PR47	30.77075000	91.60053333	4717	std	5	2.65	1	4780000	107000	LLNL3000	62.3 + 1.4 (2.2)

[a] Bold italics indicate potential outliers reported in the original publication.

[b] Exposure-ages given here are calculated using the LSDn scaling model[30].

[c] Moraines were divided into class A (well-clustered), B (moderately-clustered), and C (poorly-clustered) qualities following Blomdin et al.[28, 29].

Supplementary references

1. Edwards, M. A. & Ratschbacher, L. Seismic and aseismic weakening effects in transtension: field and microstructural observations on the mechanics and architecture of a large fault zone in SE Tibet. *Geol. Soc. Lond. Special Publ.* **245,** 109–141 (2005).
2. Pan, Y. & Kidd, W. Nyainqentanglha shear zone: A late Miocene extensional detachment in the southern Tibetan Plateau. *Geology* **20,** 775–778 (1992).
3. Benn, D. I. & Owen, L. A. The role of the Indian summer monsoon and the mid-latitude westerlies in Himalayan glaciation: review and speculative discussion. *J. Geol. Soc. (London, U. K.)* **155,** 353–363 (1998).
4. Yu, W. et al. Different region climate regimes and topography affect the changes in area and mass balance of glaciers on the north and south slopes of the same glacierized massif (the West Nyainqentanglha Range, Tibetan Plateau). *J. Hydrol.* **495,** 64–73 (2013).
5. Kuhle, M. Observations supporting the Pleistocene inland glaciation of High Asia. Results of the Sino-German Joint Expeditions (II). *GeoJournal* **25,** 133–511 (1988).
6. Xu, D. & Shen, Y. On Ancient Ice-Sheet and Ice Age in the Tibetan Plateau. *J. Glaciol. Geocryol.* **17,** 213–229 (1995).
7. Lehmkuhl, F., Klinge, M. & Lang, A. 2002. Late Quaternary glacier advances, lake level fluctuations and aeolian sedimentation in Southern Tibet. *Z. Geomorphol. Suppl.* **126,** 183–218 (2002).
8. Wu, Z., Zhao, X., Zhu, D. & Wu, Z. 2002. The moraines of Xibu Glacier Area in the Nyainqentanglha Range. *Acta Geosci. Sin.* **23,** 343–348 (2002).
9. Zhao, X., Wu, Z., Zhu, D. & Hu, D. Quaternary glaciations in the west Nyainqentanglha Mountains. *Quat. Sci.* **22,** 424–433 (2002).
10. Zhu, D. et al. The division of Quaternary glacial epochs of middle Nyainqentanglha Range. *Acta Geosci. Sin.* **23,** 335–342 (2002).
11. Zhu, D. et al. Fabric analysis of gravel in Quaternary gravel beds on backbone area of Niqinganggulashan Mountains. *J. Geomech.* **8,** 321–332 (2002).
12. Wu, Z., Zhao, X., Jiang, W., Wu, Z. & Zhu, D. Dating result of the Pleistocene Glacial Deposits on the Southeast Foot of Nyainqentanglha Mountains. *J. Glaciol. Geocryol.* **25,** 272–274 (2003).
13. Owen, L. A. et al. Climatic and topographic controls on the style and timing of Late Quaternary glaciation throughout Tibet and the Himalaya defined by ^{10}Be cosmogenic radionuclide surface exposure dating. *Quat. Sci. Rev.* **24,** 1391–1411 (2005).

14. Lisiecki, L.E. & Raymo, M.E. A Pliocene-Pleistocene stack of 57 globally distributed benthic $\delta^{18}O$ records. *Paleoceanogr. Paleoclimatol.* 20, **PA1003** (2005).

15. Clark, P. U. et al. The last glacial maximum. *Science* **325,** 710–714 (2009).

16. Chevalier, M. -L. et al. Constraints on the late Quaternary glaciations in Tibet from cosmogenic exposure ages of moraine surfaces. *Quat. Sci. Rev.* **30,** 528–554 (2011).

17. Dong, G. et al. Cosmogenic ^{10}Be surface exposure dating and glacier reconstruction for the Last Glacial Maximum in the Quemuqu Valley, western Nyainqentanglha Mountains, South Tibet. *J. Quat. Sci.* **32,** 639–652 (2017).

18. Dong, G. Yi, C. & Caffee, M. W. ^{10}Be dating of boulders on moraines from the last glacial period in the Nyainqentanglha mountains, Tibet. *Sci. China. Earth. Sci.* **57,** 221–231 (2014).

19. Xu, X. et al. Late Glacial glacier-climate modeling in two valleys on the eastern slope of Samdainkangsang Peak, Nyaiqentanggulha Mountains. *Sci. China Earth Sci.* **60,** 135–142 (2017).

20. Xu, X. et al. The effects of climatic change and inter-annual variability on glacier retreat from ~ 1850s AD moraines in the Kuoqionggangri peak region, southern Tibetan Plateau. *Clim. Dyn.* **62,** 2941–2951 (2023).

21. Zhang, L., Xu, X., Zhang, Q., Yi, C. & Zhu, Y. 2019. Glacier change in the western Nyainqentanglha Range, southern Tibet, since the Little Ice Age. *J. Earth Environ.* **10,** 567–578 (2019).

22. Xu, X. & Glasser, N. F. Glacier sensitivity to equilibrium line altitude and reconstruction for the Last Glacial cycle: glacier modeling in the Payuwang Valley, western Nyaiqentanggulha Shan, Tibetan Plateau. *Palaeogeogr. Palaeoclimatol. Palaeoecol.* **440,** 614–620 (2015).

23. Xu, X., Pan, B., Dong, G., Yi, C. & Glasser, N. F. Last Glacial climate reconstruction by exploring glacier sensitivity to climate on the southeastern slope of the western Nyaiqentanglha Shan, Tibetan Plateau. *J. Glaciol.* **63,** 361–371 (2017).

24. Li, Y. et al. Cosmogenic ^{10}Be constraints on Little Ice Age glacial advances in the eastern Tian Shan, China. *Quat. Sci. Rev.* **138,** 105–118 (2016).

25. Mangerud, J. Gosse, J. Matiouchkov, A. & Dolvik, T. Glaciers in the Polar Urals, Russia, were not much larger during the Last Global Glacial Maximum than today. *Quat. Sci. Rev.* **27,** 1047–1057 (2008).

26. Dortch, J. M. et al. A tool for the ages: The probabilistic cosmogenic age analysis tool (P-CAAT). *Quat. Geochronol.* **71,** 101323 (2022).

27. Ross, S. M. Peirce's criterion for the elimination of suspect experimental data. *J. Eng. Technol.* **20,** 38–41 (2003).

28. Blomdin, R. et al. Evaluating the timing of former glacier expansions in the Tian Shan: A key step towards robust spatial correlations. *Quat. Sci. Rev.* **153,** 78–96 (2016).

29. Blomdin, R. et al. Timing and dynamics of glaciation in the Ikh Turgen Mountains, Altai region, High Asia. *Quat. Geochronol.* **47,** 54–71 (2018).

30. Lifton, N. Sato, T. & Dunai, T. J. Scaling in situ cosmogenic nuclide production rates using analytical approximations to atmospheric cosmic-ray fluxes. *Earth Planet Sci. Lett.* **386,** 149–160 (2014).

31. Lal, D. Cosmic ray labeling of erosion surfaces: in situ nuclide production rates and erosion models. *Earth Planet Sci. Lett.* **104,** 424–439 (1991).

32. Stone, J. O. Air pressure and cosmogenic isotope production. *J. Geophys. Res.* **105,** 23753–23759 (2000).

33. Balco, G. Stone, J. O. Lifton, N. A. & Dunai, T. J. A complete and easily accessible means of calculating surface exposure ages or erosion rates from ^{10}Be and ^{26}Al measurements. *Quat. Geochronol.* **3,** 174–195 (2008).

34. Fenton, C. R. Binnie, S. A. Dunai, T. & Niedermann, S. 2022. The SPICE project: Calibrated cosmogenic ^{26}Al production rates and cross-calibrated ^{26}Al/^{10}Be, ^{26}Al/^{14}C, and ^{26}Al/^{21}Ne ratios in quartz from the SP basalt flow, AZ, USA. *Quat. Geochronol.* **67,** 101218 (2022).

35. Fenton, C. R. Niedermann, S. Dunai, T. & Binnie, S. A. The SPICE project: Production rates of cosmogenic ^{21}Ne, ^{10}Be, and ^{14}C in quartz from the 72 ka SP basalt flow, Arizona, USAu. *Quat. Geochronol.* **54,** 101019 (2019).

36. Borchers, B. et al. Geological calibration of spallation production rates in the CRONUS-Earth project. *Quat. Geochronol.* **31,** 188–198 (2016).

37. Lifton, N. Implications of two Holocene time-dependent geomagnetic models for cosmogenic nuclide production rate scaling. *Earth Planet Sci. Lett.* **433,** 257–268.

38. Putnam, A.E. Den, G.H. & Schaefer, J.M. A ^{10}Be chronology of the Esmark Moraine and Lysefjorden region, southwestern Norway: Evidence for coeval glacier resurgence in both polar hemispheres during the Antarctic Cold Reversal. *Quat. Sci. Rev.* **316,** 108259 (2023).

39. Jóhannesson, T. Raymond, C.F. & Waddington, E.D. A simple method for determining the response time of glaciers in Glacier Fluctuations

and Climatic Change (ed. Oerlemans, J.) 355–369 (1989).

40. Pellitero, R. et al. A GIS tool for automatic calculation of glacier equilibrium-line altitudes. *Comput. Geosci*. **83,** 55–62 (2015).

41. Huintjes, E. et al. Evaluation of a Coupled Snow and Energy Balance Model for Zhadang Glacier, Tibetan Plateau, Using Glaciological Measurements and Time-Lapse Photography. *Arct. Antarct. Alp. Res.* **47,** 573–590 (2015).

42. Zhu, M. Yao, T. Yang, W. Xu, B. & Wu, G. et al. Differences in mass balance behavior for three glaciers from different climatic regions on the Tibetan Plateau. *Clim. Dyn.* **50,** 3457–3484.

43. Mohtadi, M. et al. North Atlantic forcing of tropical Indian Ocean climate. *Nature* **509,** 76–80 (2014).

44. Chen, M.-T. et al. Dynamic millennial-scale climate changes in the northwestern Pacific over the past 40,000 years. *Geophys. Res. Lett.* **37,** L23603.

45. Scott, L. Poulsen, C. Lund, S. & Thunell, R. Super ENSO and Global Climate Oscillations at Millennial Time Scales. *Science* **297,** 222–226 (2002).

46. Schiau, L. et al. Warm pool hydrological and terrestrial variability near southern Papua New Guinea over the past 50k. *Geophys. Res. Lett.* **38,** L00F01 (2011).

47. Kodera, K. Solar influence on the Indian Ocean Monsoon through dynamical processes. *Geophys. Res. Lett.* **31,** GL020928 (2004).

48. Chikamoto, Y. et al. Skilful multi-year predictions of tropical trans-basin climate variability. *Nat. Commun.* **6,** 6869 (2015).

49. Nishiizumi, K. et al. Absolute calibration of ^{10}Be AMS standards. *Nucl. Instrum. Methods Phys. Res. Sect. B Beam Interact. Mater. Atoms* **258,** 403–413 (2007).